

SIMULATION OF AIRCRAFT WAKE VORTICES DURING LANDING WITH DECAY ENHANCING OBSTACLES

A. Stephan* , F. Holzäpfel* , T. Misaka**

*Deutsches Zentrum für Luft- und Raumfahrt (DLR), Institut für Physik der Atmosphäre

**Tohoku University, Institute of Fluid Science

Keywords: *Wake vortex, RANS-LES coupling, Plate line, Landing, Turbulence*

Abstract

Wake-vortex evolution during landing of a long range aircraft is investigated in a turbulent environment. The simulations cover final approach, touchdown on the tarmac, and the evolution of the wake after touchdown. An ambient turbulent crosswind and headwind field is generated in a pre-simulation. The wake is initialized using a RANS-LES coupling approach. The aircraft in high-lift configuration with deployed flaps and slats is swept through a ground fixed domain. The fuselage turbulence is modeled as white noise. The further development of the vortical wake is investigated by large-eddy simulation until final decay. After touchdown wake vortices are subjected to strong three-dimensional deformations and linkings with the ground. The downwind vortex is strongly advected with the wind and decays quickly. End effects, appear after touchdown and propagate along the wake vortices against the flight direction. They lead to a non-uniform circulation decay of the rolled-up wake vortices. Additionally the effect of a plate line installed in front of the runway is studied with this method. The plates cause disturbances of the vortices propagating to either side and interacting with the end effects. The plate line further accelerates the vortex decay.

1 Introduction

As an unavoidable consequence of lift, aircraft generate a pair of counter-rotating and long-lived wake vortices that pose a potential risk to following aircraft, due to strong coherent flow structures [1]. The probability of encountering wake vortices increases significantly during final approach in ground proximity, since rebounding vortices may not leave the flight corridor vertically and the possibility of the pilot to counteract the imposed rolling moment is restricted [2, 3]. In the recent “Challenges of growth 2013” report [4] the conceivable capacity problems of airports are elucidated. Several economic scenarios for the future European airport demands are analyzed, realizing that there will be around 1.9 million unaccommodated flights in the most-likely case, constituting approximately 12% of the demand in 2035. A reduction of the established static aircraft separation distances appears feasible employing advanced wake-vortex advisory systems (WVAS) incorporating the state-of-the-art wake-vortex physics to accurately predict vortex strength and position [5], depending on the environmental conditions. Therefore the physical mechanisms of wake-vortex evolution and decay during and after landing have to be understood.

Aircraft landing and the evolution of the wake in its meteorological environment is an example of complex turbulent flows, composed of strong coherent flow structures that exhibit

a range of length scales spanning several orders of magnitude all interacting with one another. The flow around an aircraft's main wing, fuselage, slat, flap, jet engine and tail plain, as well as the interaction with the approaching ground and the sudden lift reduction during touchdown substantially affect the generated wake vortices. Usually Reynolds-averaged Navier-Stokes (RANS) simulations are used for the flow around the aircraft and the subsequent roll-up process of the wake in the roll-up phase [6]. The dynamics of rolled-up wake vortices in ground proximity subjected to a turbulent wind have been mainly studied by large-eddy simulations (LES) [7]. This approach neglects the effects of different vortex generation heights above ground and of touchdown and may not capture full three-dimensional vortex deformations appearing during landing.

It is well known that when the vortex pair descends it induces a vorticity layer at the ground. An adverse pressure gradient builds up in the boundary layer while the primary vortices are diverging. The boundary layer finally rolls up into secondary vortices and separates [19]. From numerical simulations, as well as field measurement campaigns [3] we observe a minimum descent height of about $b_0/2$, (assuming the vortices are initialized sufficiently aloft), at the instant when secondary vortices detach from the ground.

The methodology of RANS-LES coupling enable an innovative methodology to fly a realistic aircraft through a simulation domain generating a realistic wake [8]. For this purpose, a high-fidelity steady RANS flow field is swept through the LES domain. So a spatial development of the aircraft wake is introduced in the LES. We use this approach to simulate the final approach and landing and study the physics of the wake-vortex evolution and decay. A high-lift configuration of a long range aircraft is employed to account for the landing and flare phase. Note that this approach can be viewed as a one way coupling. The changing environment, i.e. the approach of the ground is not reflected by the RANS field. This work continuous the investi-

gation in [9] including the effect of turbulence - ambient turbulence as well as fuselage turbulence. We deduce the fully three-dimensional vortex characteristics in a turbulent environment. The current study reveals that the simplified modeling fails to reproduce many characteristic flow features.

In accordance with flight practice¹ we characterize the evolution of the aircraft's wake during landing by four main phases, *Final approach*, *Flare*, *Touchdown* and *Roll-out*. Complex vortex deformations in ground proximity like vortex linking with the ground have been observed [7]. However, the effect of these structures encountered by following aircraft is not clear. We study so called end effects, appearing after touchdown, when vortex circulation is drastically reduced, as a reason that aircraft landings are safer than expected. Additionally, the interaction of end effects and disturbances caused by plate lines [10] - a method for artificial vortex decay enhancement - is investigated with the present approach. In the meanwhile first results of flight measurement campaigns at Oberpfaffenhofen airport as well as Munich airport (Germany) confirming plate line effects as well as landing effects have been presented in [11], complementing the findings in this numerical study. Results from six simulations are included in this paper, *non-turbulent*, *crosswind* and *headwind* simulations, each performed with and without the influence of a plate line.

2 Methods

2.1 Governing equations

The LES is performed using the incompressible Navier-Stokes code MGLET, developed at Technische Universität München, for solving the Navier-Stokes equa-

¹http://www.skybrary.aero/index.php/Landing_Flare?utm_source=SKYbrary&utm_campaign=47ff8e1e92-SKYbrary_Highlight_04_07_2013&utm_medium=email&utm_term=0_e405169b04-47ff8e1e92-264071565 date: June 30, 2014

tions and the continuity equation [12]

$$\frac{\partial u_i}{\partial t} + \frac{\partial(u_i u_j)}{\partial x_j} = -\frac{1}{\rho} \frac{\partial p'}{\partial x_i} + \frac{\partial}{\partial x_j} ((\mathbf{v} + \mathbf{v}_t) 2S_{ij}) \quad (1)$$

$$\frac{\partial u_j}{\partial x_j} = 0 \quad (2)$$

Here u_i represents the velocity components in three spatial directions ($i = 1, 2$, or 3), $S_{ij} = (\partial u_i / \partial x_j + \partial u_j / \partial x_i) / 2$ denotes the strain rate tensor, and $p' = p - p_0$ equals the pressure deviation from the reference state p_0 . The kinematic viscosity is given as the sum of molecular viscosity ν and eddy viscosity ν_t determined by means of a Lagrangian dynamic sub-grid scale model [13]. Equations (1) and (2) are solved by a finite-volume approach, using a fourth-order finite-volume compact scheme [14]. A split-interface algorithm is used for the parallelization of the tri-diagonal system computing coefficients of the compact scheme. A third-order Runge-Kutta method is used for time integration. The simulations are performed in parallel, using a domain decomposition approach.

The concept of artificial wake vortex decay enhancement by plate lines is also pursued in this work. A respective patent has been filed under number DE 10 2011 010 147. Figure 1 displays the arrangement of the plates in a line perpendicular to the runway. The plate line is characterized by the plate separation Δy , the height h and the plate length. The plate line is modeled by introducing a drag force source term, $-F_{D,i} = -C_D |u| u_i$, to Eq. (1) with a large drag coefficient at the plate. At the ground surface of the LES domain we employ the Grötzbach-Schumann wall model that locally computes the wall shear stress τ_w instantaneously based on the logarithmic law [15].

2.2 Ambient turbulent wind field

In order to provide a realistic environment we establish a turbulent wind in a separate simulation. We simulate a turbulent half-channel flow with $\text{Re}_\tau = 3455$ applying a free-slip condition at the top of the domain.[16] Prescribing initially a vertical wind profile following

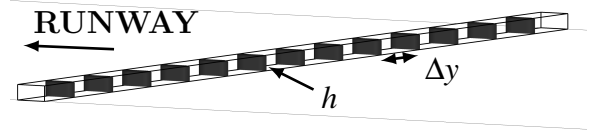


Fig. 1 Schematic representation of a plate line. Thin plates with height h and separation Δy (from [9]).

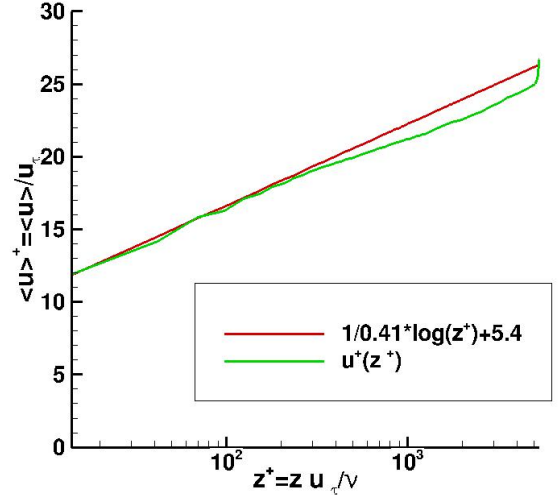


Fig. 2 Mean velocity profile characterizing the separately simulated turbulent wind.

the universal logarithmic law and imposing a stream-wise pressure gradient of $dp/dy = 1.2 \cdot 10^{-4} \text{ N/m}^3$, the wind flow is driven through the computational domain. We let the flow develop until characteristic wall streaks appear and an equilibrium between the pressure gradient and the wall friction is established. The averaged wind profile $\langle u^+ \rangle$, see Fig. 2, converge to the typical half channel flow characteristics.[16] The time-averaged stream-wise velocity of the wind at $b_0 = \frac{\pi}{4} b$ above the ground is $w_0 = 0.49 \text{ m/s}$, where w_0 is the initial vortex descent speed. Let δ denote the channel half height and consider the following quantities as averaged in time. For the boundary layer approximation the Navier-Stokes equations yield the wall shear stress $\tau_w = -\delta \cdot \partial p / \partial x$, with constant pressure in wall-normal direction. The wall friction velocity is defined by $u_\tau = (\tau_w / \rho)^{1/2}$. This yields the

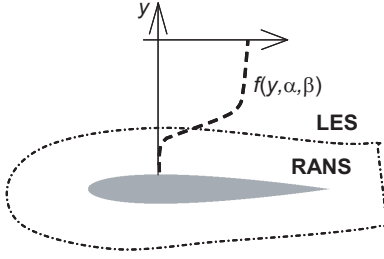


Fig. 3 Schematic of a weighting function for a combination of RANS and LES flow fields (from [8]).

normalized values $u^+ = u/u_\tau$, $z^+ = zu_\tau/\nu$ and an intrinsic Reynolds number $\text{Re}_\tau = u_\tau\delta/\nu$. The boundary layer of a turbulent flow has now three characteristic parts, the viscous sub-layer, the transition layer and the logarithmic layer, see Fig. 2.

2.3 Wake initialization

We employ a wake initialization approach where a realistic aircraft wake is generated in an LES domain by sweeping a high-fidelity steady RANS flow field through the domain, which enables the simulation of the wake-vortex evolution from generation until final decay [8]. The simulations are performed for a long range aircraft model in high-lift configuration that has been used in ONERA’s catapult facility during the European AWIATOR project. The RANS flow field serves as a forcing term of the Navier-Stokes equations in the LES. This approach might be referred to as a fortified solution algorithm [17]. The resulting velocity field in the aircraft vicinity consists of the weighted sum

$$\mathbf{V} = f(y)\mathbf{V}_{\text{LES}} + (1 - f(y))\mathbf{V}_{\text{RANS}} \quad (3)$$

of the LES and the RANS velocity field, see Fig 3, with a transition function

$$f(y, \alpha, \beta) = \frac{1}{2} \left[\tanh \left[\alpha \left(\frac{y}{\beta} - \frac{\beta}{y} \right) \right] + 1.0 \right]. \quad (4)$$

Here α and β represent slope and wall-distance of the transition, chosen similar to the values in [8]. The mapping of the RANS flow field from an unstructured, mesh refined grid

to the structured LES domain is performed by a linear interpolation conducted only once before the wake initialization. First the steady RANS solution is mapped to a Cartesian grid, a so-called frame, which is mapped to the LES grid, shifted for every time step. As the frame can only be mapped at discrete grid positions of the LES grid, a sinking glide path can not be realized by one fixed frame. For a glide path angle of 3.56 degree we employ 32 frames, prepared in advance. This requires additional memory, however, few additional computation time is needed. This hybrid method enables to study the effect of an ambient turbulent cross-wind or headwind on the aircraft wake by initializing the wake to a pre-simulated turbulent wind field.

2.4 Reproduction of turbulent fluctuations

From [18] and [10] it is evident that the transfer of turbulent fluctuation in the wake to the LES field is important for the simulation of the wake evolution. In this work we use the approach of [8]. As the eddy viscosity is modeled in the RANS computation describes the subgrid scale it cannot be reproduced by the mapped velocity field. Hence, the modeled fluctuations have to be reproduced during the mapping process.

In a straight forward approach the velocity fluctuations are modeled as white noise in the RANS-LES transition region, controlling the magnitude by the proportional-integral (PI) controller during the movement of the RANS field through the LES domain.

$$\mathbf{V}_{\text{RANS+WN}} = \mathbf{V}_{\text{RANS}} + K\mathbf{V}_{\text{WN}}, \quad (5)$$

$$K = a_1(\bar{k}_{t,\text{LES}} - k_{t,\text{RANS}}) \quad (6)$$

$$+ a_2 \int (\bar{k}_{t,\text{LES}} - k_{t,\text{RANS}}) dt, \quad (7)$$

where \mathbf{V}_{WN} denotes the white noise field and K controls the magnitude. The constants are set to $a_1 = 40$ and $a_2 = 1.0$ in the simulations including turbulence.

2.5 Computational setting

We employ a RANS flow field obtained by the DLR TAU-code from a steady compressible RANS simulation. An adaptive mesh refinement for wing-tip and flap-tip vortices, as well as the fuselage wake is employed. The flow conditions of the RANS simulation are the same as in ONERA's catapult facility experiment, i.e. chord based Reynolds number $\text{Re} = 5.2 \times 10^5$ (two orders of magnitude lower than the real aircraft flight), flight speed $U_\infty = 25 \text{ m/s}$, and a lift coefficient of $C_L = 1.4$. The 1/27 scaled model has a wingspan of 2.236m. We normalize quantities with the reference values for an elliptic load distribution [1], initial circulation, vortex spacing, vortex descent velocity, characteristic time, vorticity unit,

$$\Gamma_0 = \frac{2C_L U_\infty b}{\pi \Lambda}, \quad b_0 = \frac{\pi}{4} b, \quad w_0 = \frac{\Gamma}{2\pi b_0}, \quad (8)$$

$$t_0 = \frac{b_0}{w_0}, \quad \omega_0 = \frac{1}{t_0}, \quad (9)$$

with a wing aspect ratio of $\Lambda = 9.3$. The resulting reference values for the normalization are $\Gamma_0 = 5.36 \text{ m}^2/\text{s}$ for circulation, $b_0 = 1.756 \text{ m}$ for length, $w_0 = 0.49 \text{ m/s}$ for velocity, and $t_0 = 3.617 \text{ s}$ for time. Normalized quantities are expressed in units of the reference values in Eq. (8) and are denoted by an asterisk. We set $t = 0$ at the instant of the touchdown.

2.6 Computational domain, approach and boundary treatment

The hybrid simulation approach and the switch to pure LES (large arrow) is sketched in Fig. 4. The first part of the simulations includes the hybrid RANS/LES wake initialization until touchdown, Fig. 4 (a). The second part is a pure LES of the evolution of the aircraft wake, Fig. 4 (b). We employ periodic boundary conditions in horizontal directions, a no-slip condition at the ground and a free-slip condition at the top. The aircraft starts in the back part of the domain passes the boundary and approaches the ground. Because of the periodicity the aircraft is placed in front of the

domain in Fig. 4 (a). After touchdown the first slice of the domain is extended into the back part at the slope of the vortex and closed artificially to a horse shoe vortex, see Fig. 4 (b). This procedure effectively avoids disturbances generated at the starting point of vortex initialization. Note that wake vortex linking due to Crow instability is frequently observed in cruise altitudes and may also occur in ground proximity. In the case of a crosswind the artificial vortex closing is not applied, due to strong tilting of the vortices. Though the vortices connect after some time in the back part disturbances, so-called end effects appear.

When the landing gear touches the ground the lift ceases quickly. Then the bound vortex, i.e. the circulation around the aircraft wings, and consequently the wake vortices are strongly reduced. We model the touchdown just by removing the RANS flow field forcing term from the simulation. In the LES we employ uniform mesh spacing for all three spatial directions, with a resolution of $dx^* = dy^* = dz^* = 0.011$. Different dimensions of the complete computational domain used for wake initialization and wake development, $23.3b_0$, $5.6b_0$ to $11.6b_0$, and $2.2b_0$ in flight, spanwise and vertical directions, respectively, depending on the case, to capture the strong divergence of the vortices and the crosswind advection. The back part of the domain with a length of $5b_0$ is used for aircraft starting and the subsequent reconnection of the vortex pair by a horseshoe vortex. The aircraft passes the domain boundary at a height of $1.2b_0$. At touchdown the tail wing is at $x^* = 16.3$ whereas the plate line is centered at $x^* = 5.1$. The plates with lengths and heights of $0.2b_0 \times 0.1b_0$ are separated by $0.45b_0$, see Fig. 1. A maximum number of 400 million nodes was employed in the calculations.

3 Results

3.1 General flow field

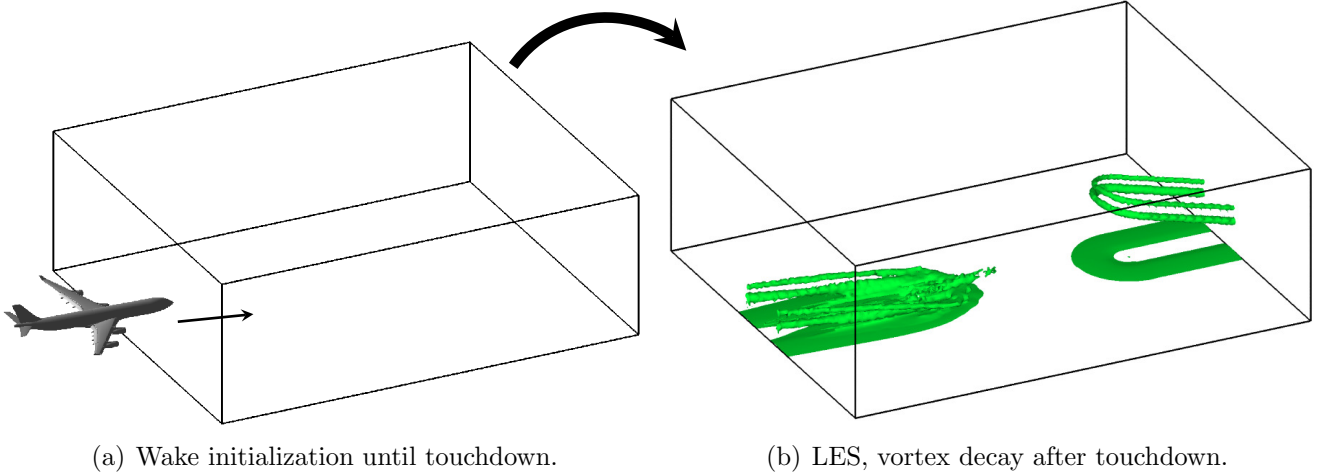


Fig. 4 Schematic of aircraft landing displaying the computational domain and the wake evolution (a) before touchdown, during wake initialization, (b) after touchdown with artificial vortex reconnection (from [9]).

3.1.1 No ambient turbulence

With this novel method we simulated the complete landing phase of an aircraft including final approach, flare, touchdown, and vortex decay [9]. Figure 5 shows the roll-up process of the aircraft wake without the influence of a wind. The tracer is initialized at certain vorticity levels, depicting the vortex structure behind the aircraft. Wing-tip and flap-tip vortices as well as a vortex from the engine pylon and from the wing fuselage junction remain at the tail wing position, as strong coherent structures. Wing-tip and flap-tip vortices merge in the mid-field constituting the so-called wake vortices. Figure 5 c) depicts the instant of touchdown. Regions of high velocities (red color), particularly dangerous for following aircraft, are around the vortex cores. After touchdown, Fig. 6, the vortices remain freely in space for a short time. At this instant so-called end effects appear from the touchdown zone, propagating against flight direction, weakening the wake vortex strength.

As vortices cannot end freely in space they tend to link with the ground. Multiple ground linkings can be observed, Fig. 6 d). The introduction of a plate line at the ground surface substantially accelerates vortex decay in the critical area close to the threshold where most vortex encounters occur, as shown in Fig. 6 c).

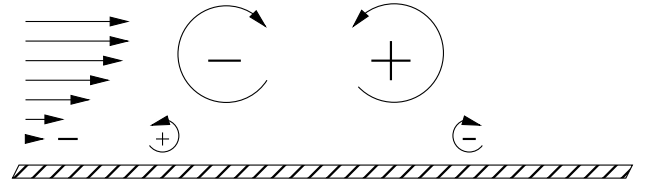


Fig. 7 Sketch of wake vortex flow with crosswind.

The reddish fraction of the vortices, indicating the potentially hazardous region, dissolves quickly.

3.1.2 Crosswind effect

The crosswind situation applying a uniform vortex initialization technique is discussed in [10]. Crosswind induces vorticity at the ground, which has opposite sign as the vorticity layer induced by the upwind vortex and the same sign as the vorticity layer induced by the downwind vortex (Fig. 7). So the crosswind vorticity supports the formation of the downwind vorticity layer and attenuates the upwind vorticity layer. As a consequence vorticity layers generated by the wake vortices become unequally strong and the upwind and downwind vortices behave asymmetrically. The magnitudes of the wake-vortex induced vorticity layers are growing leading eventually to separation and the generation

SIMULATION OF AIRCRAFT WAKE VORTICES DURING LANDING

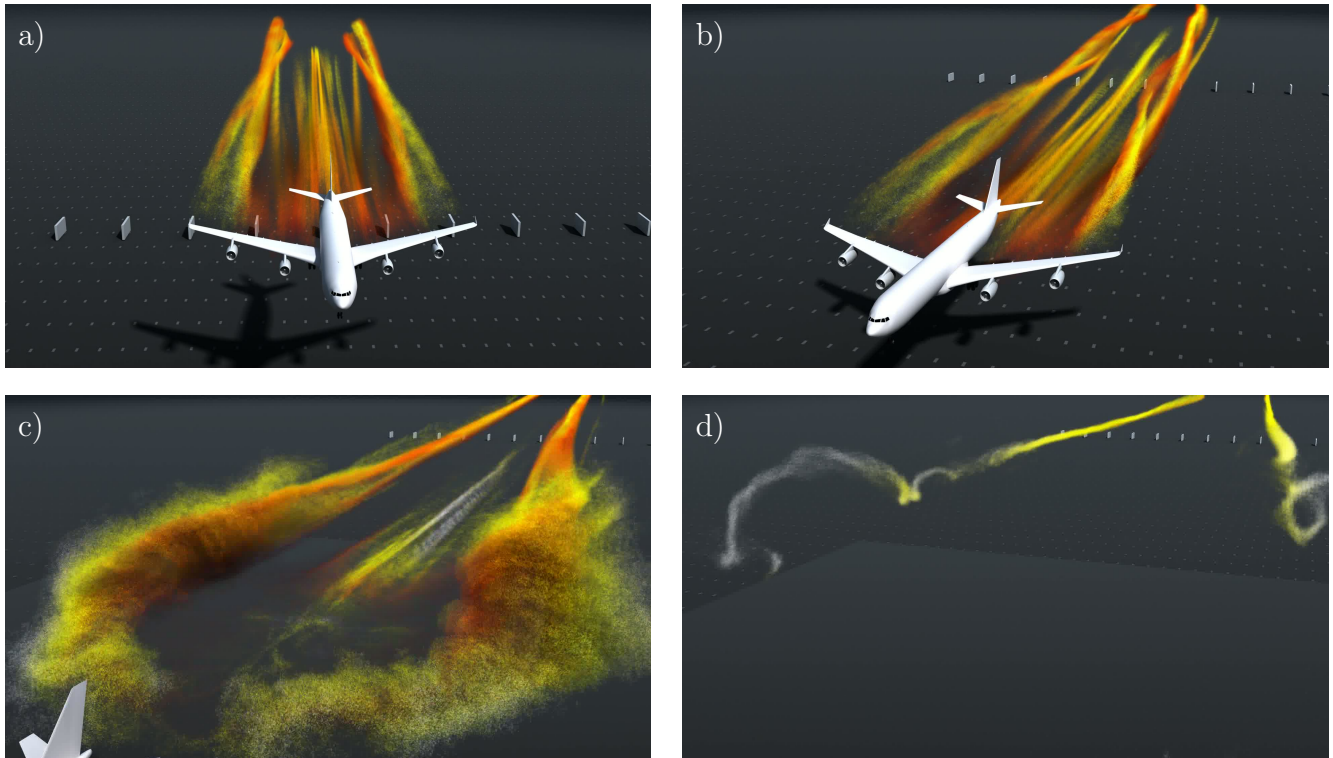


Fig. 5 Tracer Animation with Autodesk - 3d Studio MAX, (Gregor Hochleitner, Thomas Ruppert, DLR). Tracer initialized at high vorticity levels, velocity color coded. a) final approach, b) flare, c) touchdown, and d) vortex decay with end effects.

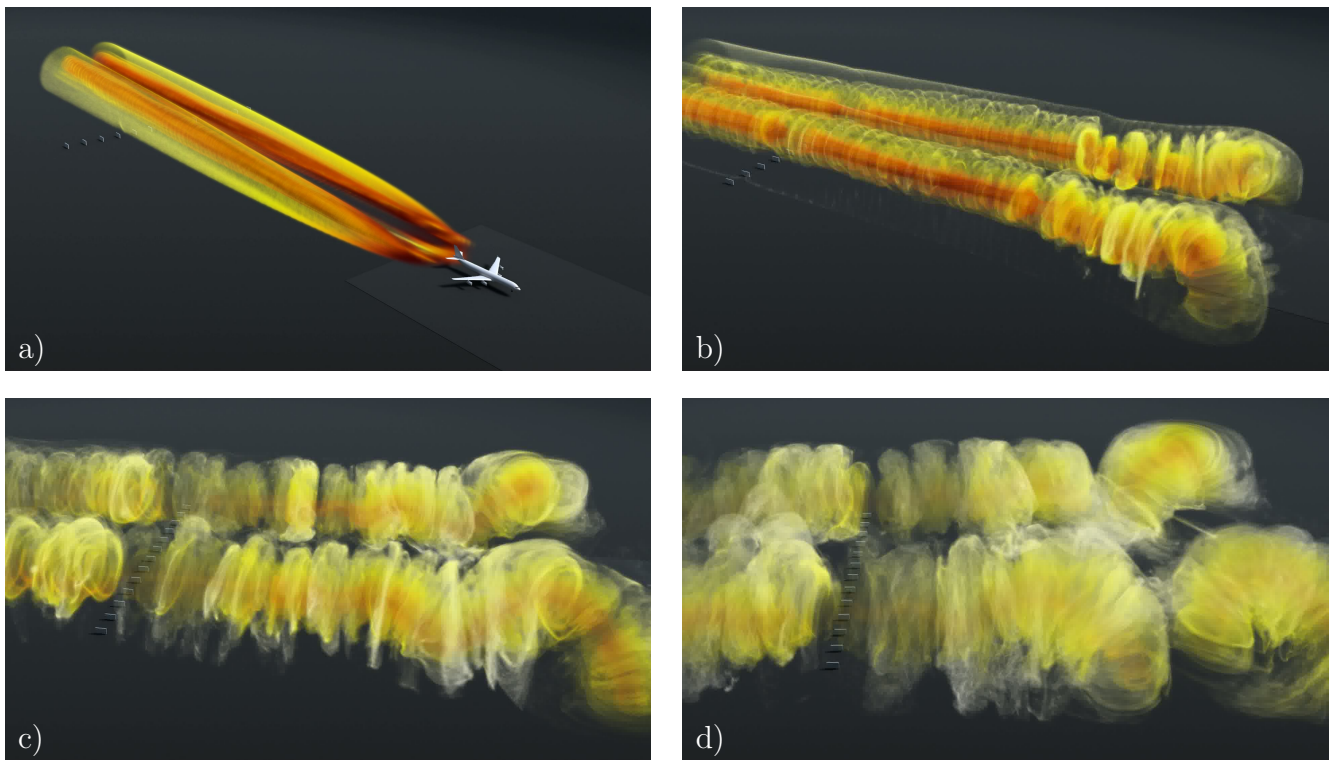


Fig. 6 Tracer Animation with Autodesk - 3d Studio MAX, (Gregor Hochleitner, Thomas Ruppert, DLR). Tracer initialized behind the aircraft, velocity color coded. a) initial wake, b) ground effect with vortex bursting, c) plate line effect and d) ground linking.

of counter-rotating secondary vortices, first at the downwind and then at the upwind vortex. Then the secondary vortices rebound and interact with the primary vortices. We observe that a tilting of the vortices may happen in the crosswind situation, see Fig. 8 a). While the downwind vortex is advected with the crosswind, the upwind vortex remains above the runway for the entire simulation time, see Fig. 8 a)-d). The ambient turbulence and favorable wind shear actively destroy the downwind vortex.

3.2 Vortex topology

The RANS-LES coupling enables to investigate the complex three-dimensional vortex deformations. Vortex linking after touchdown, see Fig. 8, and possible linking of other parts of the wake vortices reflect the complexity of the phenomenon in reality. The end effects are clearly visible, Fig. 8 (green iso-surface). Note that LIDAR measurements use to detect the velocity field in a plane perpendicular to the flight path. Measurement footprints showing cusps cannot be explained by classical theory. The stretching of the vortices and the influence of a headwind, transporting the vortices against flight direction, provide an explanation incorporating three-dimensional effects.

3.3 Vortex decay and plate line effect

As a common measure of the vortex intensity for aircraft with sufficiently large wingspans, we consider $\Gamma_{5-15} = 0.1 \int_{5\text{m}}^{15\text{m}} \Gamma(r) dr$ for the primary vortices, where $\Gamma(r) = \oint \vec{u} \cdot d\vec{s}$ denotes the circulation around a circle of radius r centered in the vortex core. Figure 9 compares head- and crosswind situation, with and without the influence of a plate line. All four figures show the end effect, starting at the point of touchdown and propagating against the flight direction. In agreement with former results the plate line considerably enforces the decay. Note that the upwind vortex in the crosswind case is tilted upwards, see Fig. 8. Therefore the interaction with the plate line starts later. The headwind case reveals a vor-

tex ground linking, leaving a horseshoe vortex which is transported with the wind, similar to Fig. 6 d).

4 Conclusion

A complete landing phase of a long range aircraft including final approach, flare, touchdown, in various ambient wind situations, and the evolution of its wake was simulated, combining RANS and LES flow fields. A RANS solution is used as a forcing term in the ground fixed LES domain. The effect of a plate line was investigated in all situations. The complex multi-scale flow field of a landing aircraft, particularly the different vortices constituting the wake are visualized and analyzed. Complex vortex interaction with the ground, end effects occurring after touchdown are investigated. They lead to rapid circulation decay. In ground proximity wake vortices are subjected to strong deformation and transport. The well known quasi two-dimensional vortex ground interaction in crosswind and/or headwind situation becomes much more complex. This yields a novel interpretation of vortex trajectory investigations in planes perpendicular to the flight path, occurring e.g. in LIDAR measurements. Vortex decay is analyzed and plate line effectiveness established in the turbulent setup.

Acknowledgments

We would like to thank Stefan Melber (Institut für Aerodynamik und Strömungstechnik, DLR-Braunschweig) for providing the RANS data of the AWIATOR long range aircraft model. We also acknowledge Airbus for the allowance to use it. We thank Michael Manhart and Florian Schwertfirm for the provision of the original version of the LES code MGLET. Computer time provided by Leibniz-Rechenzentrum (LRZ) is greatly acknowledged.

SIMULATION OF AIRCRAFT WAKE VORTICES DURING LANDING

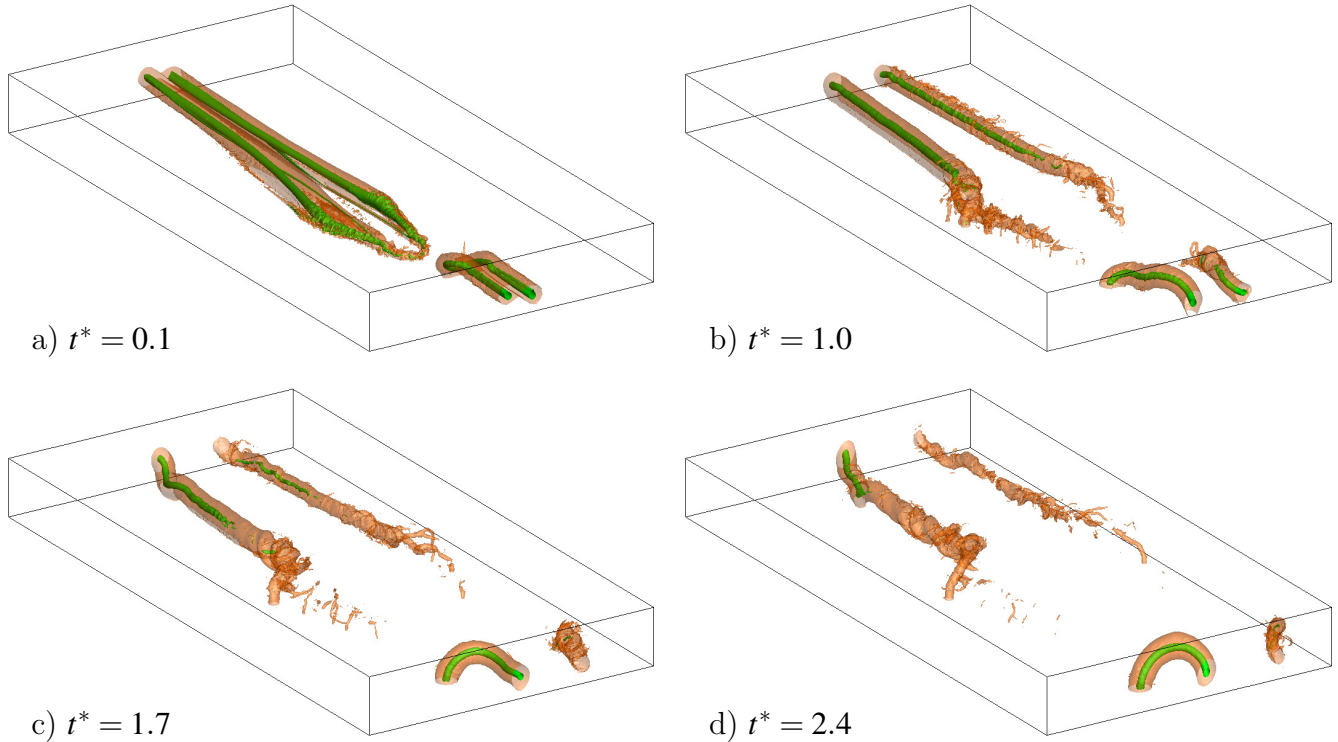


Fig. 8 Vortex topology in the crosswind case without obstacles. Two pressure iso-surfaces, -1 N/m^2 (translucent), -5 N/m^2 (green).

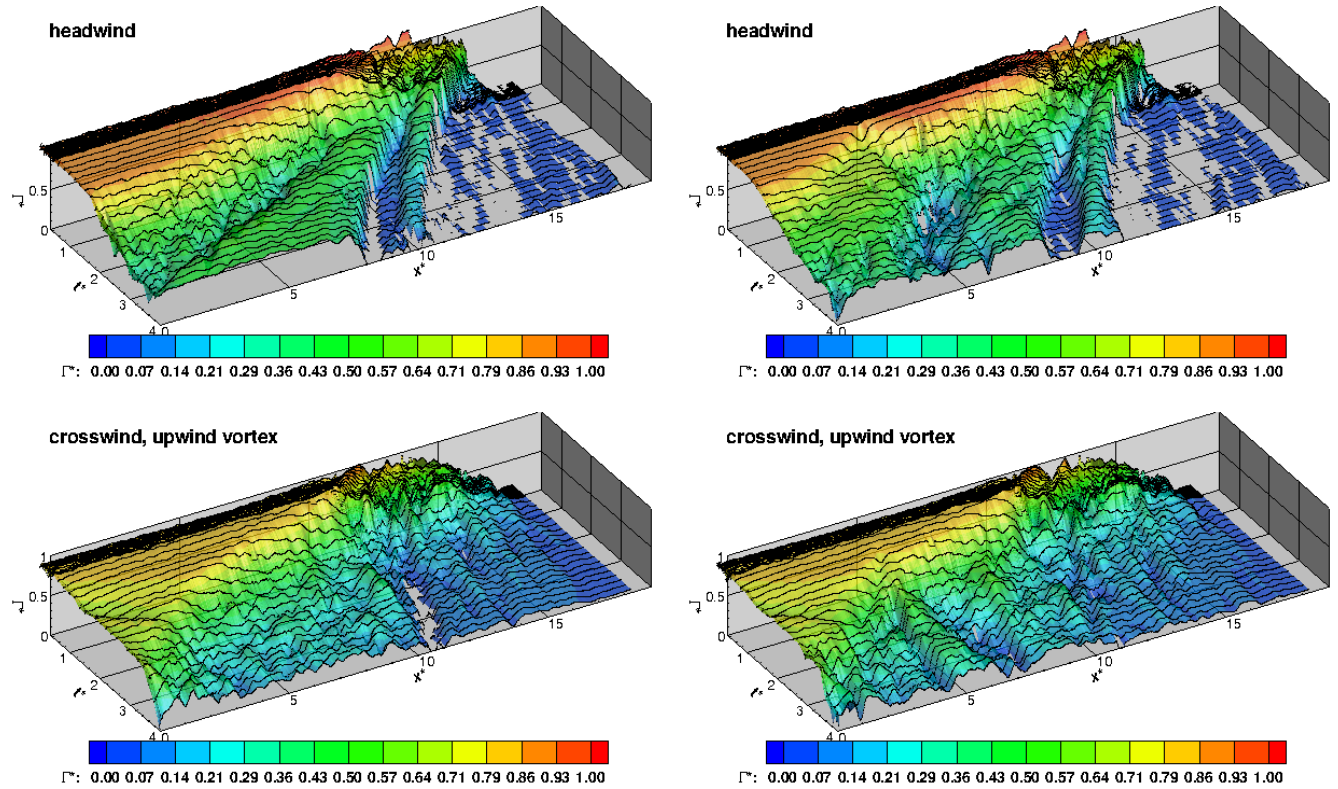


Fig. 9 Normalized vortex circulation development for the entire upwind vortex, headwind case (up), crosswind case (down), without plate line (left), plate line (right).

References

- [1] Gerz T, Holzäpfel F and Darracq D. Commercial aircraft wake vortices. Progress in Aerospace Sciences, Vol. 38, pp 181-208, 2001.
- [2] Critchley J and Foot P. UK CAA wake vortex database: Analysis of incidents reported between 1982 and 1990. Civil Aviation Authority, CAA Paper, Vol. 91, 1991.
- [3] Holzäpfel, F. and Steen, M. Aircraft Wake-Vortex Evolution in Ground Proximity: Analysis and Parametrization. AIAA Journal, Vol. 45, pp 218-227, 2007.
- [4] Eurocontrol. Challenges of growth. Summary Report, 2013.
- [5] Holzäpfel F, Gerz T, Frech M, Tafferner A, Köpp F, Smalikho I, Rahm S, Hahn K-U and Schwarz C. The Wake Vortex Prediction and Monitoring System WSVBS - Part I: Design. Air Traffic Control Quarterly, Vol. 17, No. 4, 2009
- [6] Stumpf E. Study of Four-Vortex Aircraft Wakes and Layout of Corresponding Aircraft Configurations. Journal of Aircraft, Vol. 42, pp 722-730, 2005
- [7] Proctor F H, Hamilton D W and Han J. Wake Vortex Transport and Decay in Ground Effect: Vortex Linking with the Ground AIAA, 2000-0757, 38th Aerospace Sciences Meeting & Exhibit, Reno. 2000.
- [8] Misaka T, Holzäpfel F and Gerz T. Wake Evolution of High-Lift Configuration from Roll-Up to Vortex decay. AIAA Paper 2013-0362, 51st AIAA Aerospace Sciences Meeting, Grapevine, Texas, USA, 2013.
- [9] Stephan A, Holzäpfel F, and Misaka T. Hybrid Simulation of Wake-Vortex Evolution During Landing on Flat Terrain and with Plate Line. Journal title: International Journal of Heat and Fluid Flow, DOI: 10.1016/j.ijheatfluidflow.2014.05.004
- [10] Stephan A, Holzäpfel F, and Misaka T. Aircraft Wake Vortex Decay in Ground Proximity - Physical Mechanisms and Artificial Enhancement. Journal of Aircraft, Vol. 50, No. 4, pp 1250-1260, 2013.
- [11] Holzäpfel F, Stephan A, Körner S. and Misaka T., Wake Vortex Evolution during Approach and Landing With and Without Plate Lines, 52nd Aerospace Sciences Meeting, No. AIAA 2014-0925, 2014
- [12] Manhart M. A Zonal Grid Algorithm for DNS of Turbulent Boundary Layer. Computer and Fluids Vol. 33, No. 3, pp 435-461, 2004.
- [13] Meneveau C, Lund T S and Cabot W H. A Lagrangian dynamic subgrid-scale model of turbulence. Journal of Fluid Mechanics, Vol. 319, pp 353-385, 1996.
- [14] Hokpunna A and Manhart M. Compact Fourth-order Finite Volume Method for Numerical Solutions of Navier-Stokes Equations on Staggered Grids. Journal of Computational Physics, Vol. 229, No. 20, pp 7545-7570, 2010
- [15] Grötzbach G. Direct numerical and large eddy simulations of turbulent channel flows. Encyclopedia of fluid mechanics (ed. N. Chermisinoff), 1987.
- [16] Moser R D, Kim J and Mansour N N. Direct numerical simulation of turbulent channel flow up to $Re=590$, Physics of Fluids, Vol. 11, No. 4, pp 943-945, 1991.
- [17] Fujii K. Unified Zonal Method Based on the Fortified Solution Algorithm. Journal of Computational Physics, Vol. 118, pp 92-108, 1995.
- [18] Czech M J, Miller G D, Crouch J D and Strelets M, Near-field Evolution of Trailing Vortices Behind Aircraft with Flaps Deployed. AIAA Paper 2004-2149, 2004.
- [19] Doligalski T L, Smith C R and Walker J D A. Vortex interactions with walls. Annual Review of Fluid Mechanics, Vol. 26, pp 573-616, 1994

Copyright Statement

The authors confirm that they, and/or their company or organization, hold copyright on all of the original material included in this paper. The authors also confirm that they have obtained permission, from the copyright holder of any third party material included in this paper, to publish it as part of their paper. The authors confirm that they give permission, or have obtained permission from the copyright holder of this paper, for the publication and distribution of this paper as part of the ICAS 2014 proceedings or as individual off-prints from the proceedings.